

# A solid oxide carbon fuel cell operating on pomelo peel char with high power output

Wenting An<sup>1,2</sup>  | Xiaojie Sun<sup>1</sup> | Yong Jiao<sup>1,2</sup>  | Paulo Sérgio Barros Julião<sup>2</sup> | Wei Wang<sup>2</sup> | Songbai Wang<sup>1</sup> | Si-Dian Li<sup>1</sup> | Shaomin Shuang<sup>1</sup>

<sup>1</sup>College of Chemistry and Chemical Engineering, Institute of Molecular Science, Shanxi Key Laboratory of Materials for Energy Conversion and Storage, Shanxi University, 92 Wucheng Road, Taiyuan 030006, China

<sup>2</sup>Department of Chemical Engineering, Curtin University, Perth, WA 6845, Australia

## Correspondence

Wenting An, College of Chemistry and Chemical Engineering, Shanxi University, 92 Wucheng Road, Taiyuan 030006, China; Department of Chemical Engineering, Curtin University, Perth, WA 6845, Australia.  
Email: wtan@sxu.edu.cn; wenting.an@curtin.edu.au

## Summary

The pomelo peel char (PC) was prepared and used as fuel for solid oxide electrolyte direct carbon fuel cells with nickel-yttrium stabilized zirconia anode, thin-film YSZ electrolyte, and  $\text{La}_{0.8}\text{Sr}_{0.2}\text{MnO}_3$  cathode. The power densities of fuel cells operating on PC and catalyst-loaded PC (PCC) fuels achieved 309 and 518  $\text{mW cm}^{-2}$  at 850°C, respectively, which are among the highest power densities reported in the literature on DCFCs. The PC exhibited superior gasification reactivity than coal char due to its unique reticulated foam carbon structure with a homogeneously distributed inherent catalyst. The stability tests at a current density of 50  $\text{mA cm}^{-2}$  and 825°C indicate that the cell using PC fuel operated in a more stable manner than that using PCC, and the fuel availabilities for PC and PCC were 47.25% and 34.71%, respectively. The results suggest that PC is a promising solid carbonaceous fuel for solid oxide electrolyte direct carbon fuel cells based on its adequate gasification reactivity and high compatibility with the fuel cells.

## KEYWORDS

Boudouard gasification, direct carbon fuel cell, high power output, inherent catalyst, pomelo peel biochar, reticulated foam carbon, solid oxide electrolyte

## 1 | INTRODUCTION

Direct carbon fuel cells (DCFCs) are emerging power generation technologies that promise direct and efficient conversion of the chemical energy in solid carbonaceous fuels into electrical energy.<sup>1-3</sup> The direct electrochemical conversion of carbon in DCFCs offers inherently high theoretical and practical efficiencies close to ~100% and ~80%, respectively. In contrast, the thermochemical conversion of carbon to electricity is a multistep process

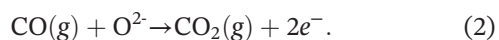
constrained by the Carnot cycle, just providing ~50% and ~40% conversion efficiencies in thermodynamics and thermal power plants, respectively.<sup>4,5</sup> Meanwhile, DCFCs have the superiority to produce concentrated  $\text{CO}_2$  product streams, which could be available for industrial use or sequestration without expensive gas separation and energy intensive purification processes.<sup>6</sup> In addition, DCFCs have the prominent benefit of fuel flexibility, allowing the use of abundant solid carbonaceous reserves in the world.<sup>7</sup> In short, DCFCs promise to

**Funding information:** Australian Research Council, Grant/Award Number: DP150104365; DP160104835; Curtin University and the China Scholarship Council, Grant/Award Number: 201608140134; Shanxi Program for the Sci-tech Activities of Returnee Scholars, Grant/Award Number: 2014; Shanxi Coal-bed Methane Joint Foundation, Grant/Award Number: 2015012016; Shanxi Natural Science Foundation, Grant/Award Number: 201601D102014; Shanxi Key Technologies R&D Program, Grant/Award Number: 20150313003-3

efficiently use carbon fuels for power generation with reduced carbon footprint.

However, DCFCs face a primary challenge of how to effectively deliver the solid carbon particles through the pores of anode to the electrochemically reactive sites on the anode/electrolyte interface.<sup>6</sup> To solve this solid-to-solid contact problem, a series of strategies have been proposed and demonstrated, such as using molten hydroxide or carbonate as electrolyte, and molten metals (eg, iron, copper, lead, indium, bismuth, antimony, and tin) as anode.<sup>2-5</sup> In addition, the hybrid type of DCFC combines a solid oxide electrolyte and a molten carbonate electrolyte to achieve better performances.<sup>2</sup> In fact, this molten media strategy faces new challenges, including the stability problem, the chemical compatibility of the molten media with other solid cell components. On the other hand, the feasibility of solid oxide electrolyte DCFCs (SO-DCFCs) has been demonstrated by integrating with an in situ catalytic Boudouard gasification of solid carbon fuels.<sup>8-12</sup> A lot of efforts have been devoted to illustrating the anode reaction mechanisms and the vital factors determining the performance of SO-DCFCs.<sup>13-15</sup>

The Boudouard gasification reactivity of solid carbon is one of the most important factors determining the performance of SO-DCFCs. In general, the reverse Boudouard reaction (the Equation (1)), or called as Boudouard gasification, is thermodynamically favored at elevated temperatures ( $\geq 1000$  K) according to the Gibbs free energy calculation.<sup>6</sup> Under the equilibrium condition at 1000 K, the partial pressure of CO is nearly 0.71 atm with a total system pressure of 1 atm. However, the use of catalysts can largely accelerate the reaction rate and reduce the initial reaction temperature.<sup>12-16</sup> The physicochemical properties of solid carbonaceous fuels also have a marked impact on their Boudouard gasification reactivity.<sup>17-20</sup> According to the anode reaction mechanism of SO-DCFCs, the reactions (1) and (2) are coupled each other, where the reaction (1) supplies CO fuel to the anode, and the fuel is electrochemically oxidized with the production of CO<sub>2</sub>. To achieve high cell performance, it is important to tune the Boudouard gasification reactivity of solid carbon fuels to match the anode needs.



Recently, the use of biomass-derived solid carbons (biochars) as fuel for SO-DCFCs has drawn growing attentions for the availability and renewability of biomass.<sup>21-25</sup> There has been a consensus that the physicochemical properties of solid carbonaceous fuels, such

as crystal structure, surface functional groups, surface area, particle size, and impurities, are important factors influencing the electrochemical performance of SO-DCFCs.<sup>2</sup> In general, biochars have unique physicochemical properties, such as textural structures and inherent catalytic constituents, which enable the fuel cells to exhibit high performances. For example, the fuel cells with different configurations operating on corn cob biochar achieved the maximum power output of 185 and 204 mW cm<sup>-2</sup> at 750°C and 800°C, respectively.<sup>26,27</sup> The surface morphology of the biochar is featured by the large pores with many smaller pores on their walls, which enlarge the surface area and provide more electrochemical/gasification reaction sites. A DC-SOFC running on a biochar derived from orchid tree leaves showed relative high performance, which stemmed from the porous structure and the catalytic effect of the uniformly distributed chemical elements.<sup>19</sup> However, biochars derived from different kinds of biomass should be diverse not only in their microstructures but also in the contained chemical elements with catalytic activity. Their effects on the performance of SO-DCFCs are worthy to study to develop new solid carbonaceous fuels with high Boudouard gasification performance.

The pomelo (*Citrus maxima*) is one of the largest underused citrus fruits with rich nutrients and certain medicinal ingredients.<sup>28</sup> Meanwhile, pomelo has more peels than most of other fruits and can potentially generate a significant amount of waste. In fact, pomelo peel (PP) is a kind of biomass resource that contains a variety of bioactive ingredients with high medicinal value, such as pectin, essential oil, and pigment. It also has abundant cellulose as the main constituent of the white flocculent layer, which is a potential precursor to fabricate carbonaceous material with essential applications in various fields, such as adsorption materials for heavy metal treatment (including uranium and other key nuclides), catalysis, and energy conversion and storage.<sup>29-33</sup> Recently, the PP-based carbonaceous materials have been developed with applications in lithium/sodium batteries, microbial fuel cells, and supercapacitors with excellent electrochemical performance.<sup>31-37</sup>

Despite the available renewability and the potential applicability, to the best of our knowledge, this is the first study on the feasibility of PP biochar as fuel for SO-DCFCs. The physicochemical properties of the biochar were fully characterized. The electrochemical performance of SO-DCFCs fed with the biochar was investigated in detail. Our goal is to improve the use of deserted biomass resources and to develop a cost-effective and high-performance solid carbon fuel compatible with SO-DCFCs.

## 2 | EXPERIMENTAL

### 2.1 | Preparation of carbon fuels

Raw pomelo peel (denoted as RP) was washed by deionized water and cut into pieces of around  $2 \times 2 \text{ cm}^2$ , then dried in oven at  $110^\circ\text{C}$  overnight. The dried RP sample was heated to  $500^\circ\text{C}$  with a uniform rate in 100 minutes in tube furnace under nitrogen atmosphere and held for 1 hour to pyrolysis completely. When cooling off to room temperature, the as-prepared PC was ground and sieved through a 200 mesh sieve. The biochar yield of PC is about 33.3 wt.%, which is the weight ratio of PC to RP. The preparation process is illustrated schematically in Figure 1. A Boudouard gasification catalyst,  $\text{Fe}_m\text{O}_n\text{-M}_x\text{O}$ , was loaded on the PC sample by impregnation method, where  $\text{M}_x\text{O}$  is a mixture of  $\text{Li}_2\text{O}$ ,  $\text{K}_2\text{O}$ , and  $\text{CaO}$ .<sup>18</sup> First, the PC sample was dispersed in the solution of  $\text{Fe}(\text{NO}_3)_3 \cdot 9\text{H}_2\text{O}$ ,  $\text{LiNO}_3$ ,  $\text{KNO}_3$ , and  $\text{Ca}(\text{NO}_3)_2$  with the molar ratio of C:Fe:Li:K:Ca = 420:6:2:2:3. The colloid was dried at  $110^\circ\text{C}$  for 12 hours and then calcined at  $700^\circ\text{C}$  for 2 hours under argon flow of  $30 \text{ mL min}^{-1}$  and then cooled down to ambient temperature in argon atmosphere. The catalyst-loaded PC is denoted as PCC, which contains approximate 21.6 wt % of the catalyst.

### 2.2 | Characterization of carbon fuels

The morphologies and the element composition analyses of carbon samples, as well as the amount of carbon deposition over the anode surface after the stability test of fuel cells, were observed using scanning electron microscopy (SEM, S-4800, Hitachi, Japan) with an embedded energy



**FIGURE 1** Schematic diagram of the preparation of pomelo peel char [Colour figure can be viewed at [wileyonlinelibrary.com](http://wileyonlinelibrary.com)]

dispersive X-ray analyzer (EDX). An automated adsorption apparatus (Micromeritics Tristar, Micromeritics, USA) was used to analyze the surface characteristics of PC by using nitrogen gas physisorption at 77 K. The specific surface area was calculated by using the Brunauer-Emmett-Teller method from adsorption data in the relative pressure ( $P/P_0$ ) range of 0.05 to 0.3. X-ray diffraction (XRD, D8 Advance diffractometer, Bruker, Germany, operated at 40 kV, 100 mA,  $\text{Cu K}\alpha$  radiation) was performed over a range of  $10$  to  $90^\circ$  to evaluate the crystalline structure of carbon samples. The quantitative crystalline parameters, including the interplanar spacing ( $d_{002}$ ), the average diameter ( $L_a$ ), and the stacking height ( $L_c$ ), are calculated by the Equation (3) and the Scherrer equation (4)<sup>17</sup>:

$$d_{002} = \frac{\lambda}{2 \sin(\theta_{002})}, \quad (3)$$

$$L = \frac{K\lambda}{\beta \cos\theta}, \quad (4)$$

where  $\lambda$  is the wavelength of the X-ray,  $\theta$  is the diffraction angle,  $\theta_{002}$  is the angle of the (002) peak,  $d_{002}$  is the crystalline interplanar spacing, and  $K$  is the peak width at the half-maximum intensity of the (002) or (100) peak.

The surface chemical properties of samples were determined by Fourier transform infrared (FTIR) spectrometer (Vertex 70, Bruker, Germany) with a resolution of  $4 \text{ cm}^{-1}$  and 32 scans between  $4000$  and  $400 \text{ cm}^{-1}$ . The thermogravimetric (TG) and differential scanning calorimetric (DSC) analyses of samples were performed simultaneously by using a bifunctional thermal analyzer (TGA/DSC I model, Mettler Toledo, Switzerland) under the identical conditions of heating 20 mg samples with a heating rate of  $10^\circ\text{C min}^{-1}$  from  $45^\circ\text{C}$  to  $1000^\circ\text{C}$  under dry air flow of  $30 \text{ mL min}^{-1}$ . The proximate and ultimate analyses of RP sample were tested by Shanxi Institute of Coal Chemistry, Chinese Academy of Science.

The Boudouard gasification reactivity of carbon samples were evaluated by using carbon dioxide temperature-programmed oxidation ( $\text{CO}_2\text{-TPO}$ ) method.<sup>18</sup> The PC sample of 30 mg and PCC of 35 mg were individually introduced into a quartz U-shape tube reactor with an inner diameter of 3 mm. The sample was first heated to  $200^\circ\text{C}$  and held for 1 hour to remove adsorbed water, and then  $\text{CO}_2$  flowed over it with a rate of  $15 \text{ mL min}^{-1}$ . The temperature further increased to  $1000^\circ\text{C}$  at a heating rate of  $10^\circ\text{C min}^{-1}$ , and the effluent gas was fed into a Hiden QIC-20 mass spectrometer to monitor the concentration of CO. The furnace temperature was

maintained at 1000°C until the CO signal returned to the baseline.

### 2.3 | Fabrication and performance test of fuel cells

Ni-YSZ (yttrium stabilized zirconia) anode-supported fuel cells with thin-film YSZ electrolyte and porous  $\text{La}_{0.8}\text{Sr}_{0.2}\text{MnO}_3$  (LSM) cathode were fabricated by using a literature procedure.<sup>38</sup> The microstructures of the as-prepared fuel cells are shown in Figure 2. The cathode and anode are porous and structurally uniform. The cross section indicates that the YSZ electrolyte is thin, uniform, and quite dense, which guarantees the gas-tight and high output of the fuel cell.

The button cell was sealed onto a quartz tube by silver paste, and the solid carbon fuel of 0.1 g was placed in intimate contact with the anode surface using asbestos to support. Two quartz tubes were positioned beneath the asbestos: one was assigned to feed in the  $\text{H}_2/\text{Ar}/\text{CO}_2$  and the other to release the reaction products. The electrochemical performance of the fuel cell was tested by using the setup schematically shown in Figure 3, where the cathode was directly exposed to air. The cell performance, including current-voltage (I-V) and electrochemical impedance spectra data, was tested by 4-terminal configuration with Iviumstat electrochemical analyzer (Ivium Technologies B.V., Netherlands).

## 3 | RESULTS AND DISCUSSION

### 3.1 | Evaluation of gasification reactivity

#### 3.1.1 | Gasification reactivity in air

Thermogravimetric and DSC curves of PC and coal char (CC) samples are depicted in Figure 4. Both the TG and DSC data indicate that there is a significant difference of the gasification reactivity in air between CC and PC. The weight loss curve of PC in Figure 4A can be divided into 4 sections as follows: (1) With the temperature increasing from 45 to 150°C, the TG plot displayed a weight loss of 5% due to water desorption. (2) With the temperature increasing from 150°C to 380°C, there was a weight loss of 22.4% with slow weight loss rates ( $\sim 0.1 \text{ wt.}\% \text{ }^\circ\text{C}^{-1}$ ), indicating the gasification of the atoms with high reactivity, such as oxygenated carbon groups. (3) In the temperature range from 380°C to 530°C, a quick weight loss of 59.2% occurred ( $\sim 0.395 \text{ wt.}\% \text{ }^\circ\text{C}^{-1}$ ), indicating a violent oxidation of the bulk carbon. (4) Finally, the mass was almost constant at temperature higher than 530°C, indicating that the

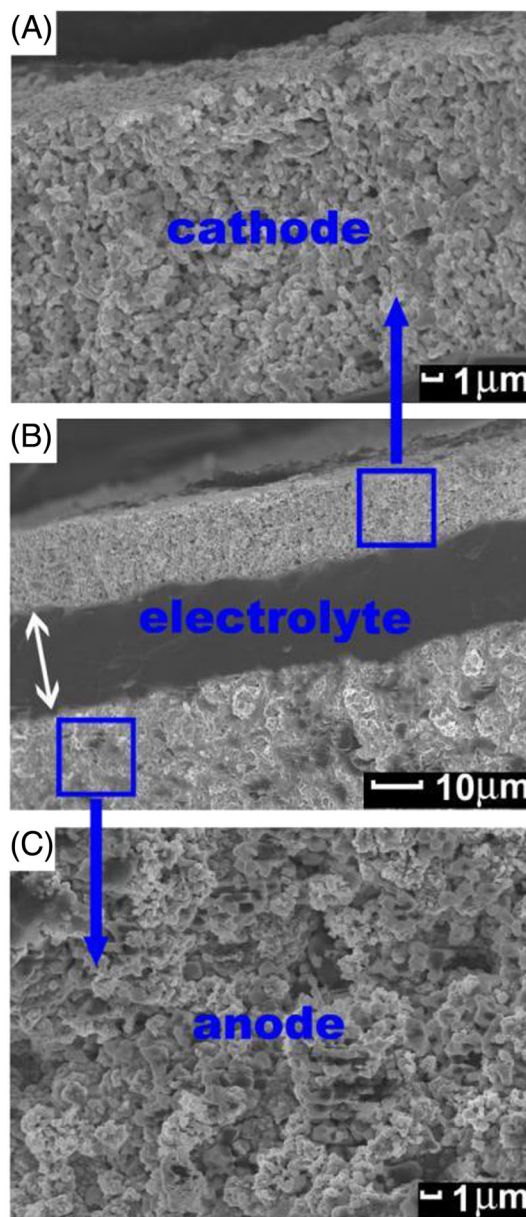


**FIGURE 2** Scanning electron microscopy images of the cell microstructure: (A) Ni-YSZ anode, (B) cross section, and (C) LSM-YSZ cathode [Colour figure can be viewed at [wileyonlinelibrary.com](http://wileyonlinelibrary.com)]

gasification process had finished and the residue was ash content with a slight decrease of the weight ratio from 13.4% to 8.6%. Regarding the weight loss curve of CC in Figure 4B, 3 sections are easily defined to describe its behavior with the increasing temperature: (1) There was almost no weight loss ( $\leq 1\%$ ) when the temperatures are less than 600°C, indicating that the gasification reactivity of CC at low temperature was very poor. (2) In the temperature range from 600°C to 955°C, there was a markedly weight loss of 83% ( $\sim 0.234 \text{ wt.}\% \text{ }^\circ\text{C}^{-1}$ ), indicating the oxidation of the bulk carbon. (3) Then the mass was almost constant when the temperatures

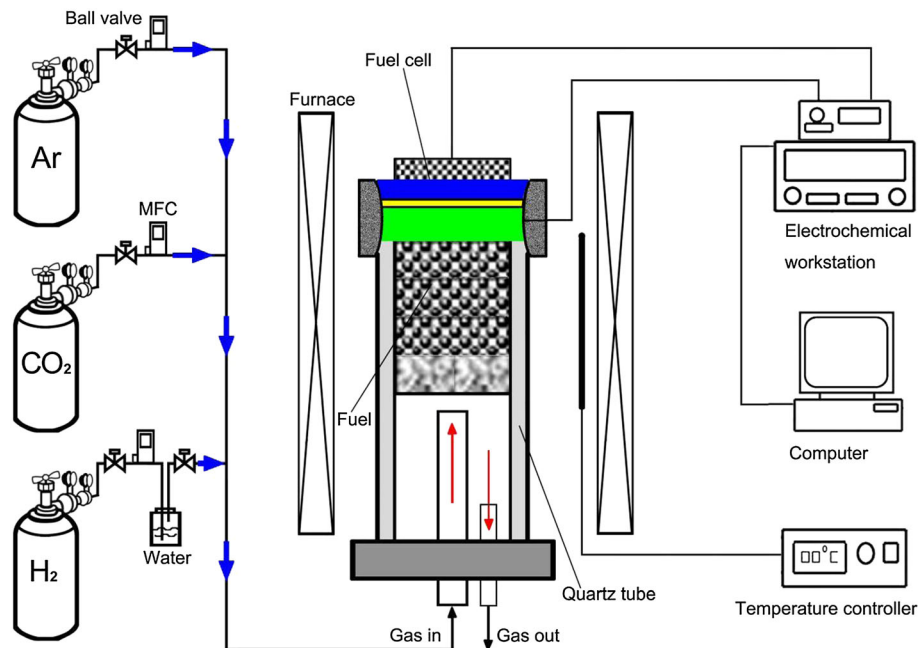


FIGURE 3 Schematic diagram of the fuel cell test setup [Colour figure can be viewed at wileyonlinelibrary.com]

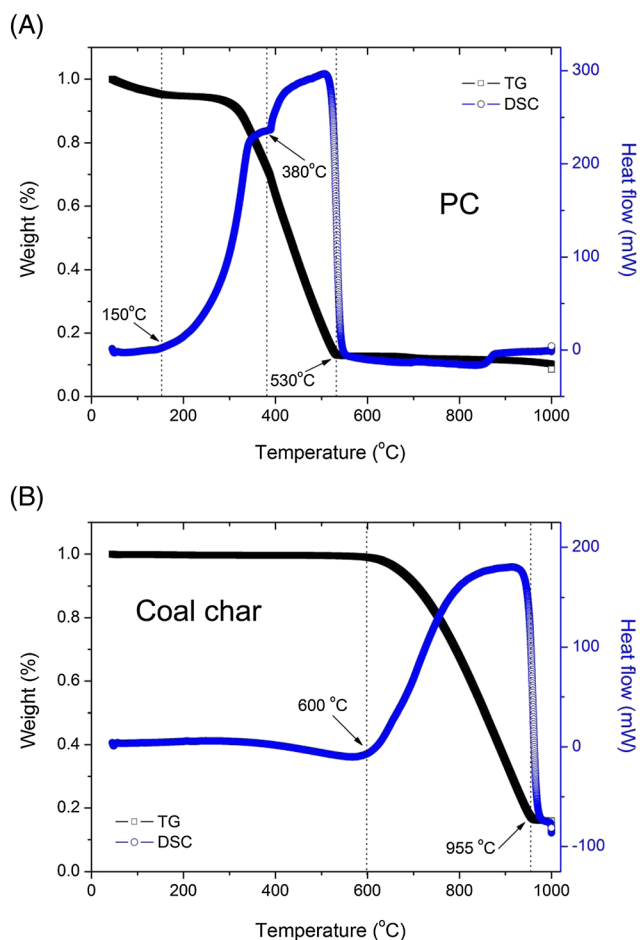


FIGURE 4 Thermogravimetric and differential scanning calorimetric profiles of (A) pomelo peel char (PC) and (B) coal char samples [Colour figure can be viewed at wileyonlinelibrary.com]

are higher than 955°C, leaving the ash content with a weight ratio of ~16%.

The DSC curves in Figure 4A,B show the heat flow characteristics of PC and CC samples. As listed in Table 1, the initial and end gasification temperatures, and the maximum heat flow temperature of PC, are lower 450, 425, and 410°C than those of CC, respectively. The maximum heat flow value of PC is larger 115 mW than that of CC. Therefore, PC has much higher gasification reactivity in air than CC.

### 3.1.2 | Boudouard gasification reactivity

Carbon dioxide temperature-programmed oxidation (CO<sub>2</sub>-TPO) was used to evaluate the Boudouard reactivity of PC and PCC, and the results are shown in Figure 5. The initial Boudouard reaction temperature of PC is ~591°C, which is ~195°C lower than that of an activated carbon sample (~786°C), indicating that PC is more prone to gasification under lower temperatures.<sup>18</sup> Upon impregnating PC with the Boudouard reaction catalyst to obtain PCC, its initial Boudouard gasification temperature decreased to 500°C, which is of 133°C lower than that of the catalyst-loaded activated carbon (633°C) under the identical experimental condition.<sup>18</sup> The result indicates that PC has an excellent Boudouard gasification reactivity at lower temperatures (<800°C), which should stem from the unique microstructure and the inherent catalytic matter of PC as discussed below in section 3.5. As shown in Figure 5, the Boudouard reactivity of PCC is higher than that of PC in the whole temperature range

**TABLE 1** Information extracted from the differential scanning calorimetric curves

	Initial Gasification Temperature, °C	End Gasification Temperature, °C	Maximum Heat Flow, mW	Maximum Heat Flow Temperature, °C
Pomelo peel char	150	550	295	505
Coal char	600	975	180	915

from 500°C to 1000°C, although the superiority is limited. At 850°C, one of the typical operating temperatures for the SO-DCFCs, the CO intensity of PCC ( $3.08 \times 10^{-7}$  torr) is approximately 1.4 times that of PC. Therefore, it was expected that the output of fuel cells fed with PCC would be higher than that of PC due to more fuels being supplied to the anode.

### 3.2 | Power output

Figure 6A,B shows the power densities of fuel cells fed with PC and PCC, which achieved 309 and 518 mW cm<sup>-2</sup> at 850°C, respectively. They belong to the highest power outputs reported in the literature of DCFCs.<sup>2</sup> So far as the biochar used as fuel for SO-DCFCs is concerned, to the best of our knowledge, PC has given the highest power output up to now. The performance results are summarized in Table 2.

As a contrast, in our previous work of using CC and catalyst-loaded CC as fuel, the peak power densities (PPDs) of fuel cells reached 100 and 204 mW cm<sup>-2</sup> at 850°C, respectively.<sup>18</sup> In particular, at the relative lower temperature, ie, 800°C, the PPDs of using CC and catalyst-loaded CC just reached 25 and 67 mW cm<sup>-2</sup>, respectively.<sup>18</sup> However, when PC and PCC were used as fuel for the fuel cells operating at 800°C, the PPDs achieved 205 and 342 mW cm<sup>-2</sup>, respectively, which are 8 and 5 times of the PPDs of the fuel cells using CC and catalyst-loaded CC as fuel, respectively. In short, the PPD

of pure PC at 800°C (205 mW cm<sup>-2</sup>) is equivalent to that of the catalyst-loaded CC at 850°C (204 mW cm<sup>-2</sup>).<sup>18</sup> It was reported that the SO-DCFCs operating on the pure corn cob char achieved 204 mW cm<sup>-2</sup> or achieved 270 mW cm<sup>-2</sup> when a Fe-based catalyst was loaded at 800°C.<sup>27</sup> In addition, a SOFC fed with the orchid tree leaf char had a PPD of 212 mW cm<sup>-2</sup> at 850°C.<sup>19</sup> When comparing with the catalyst-loaded activated carbon fuels, Shao et al reported a PPD of ~297 mW cm<sup>-2</sup> at 850°C for an anode-supported SOFC with scandium-stabilized zirconia electrolyte and a LSM cathode.<sup>13</sup> Liu et al demonstrated that a single cell and a 3-cell-stack operating on the Fe catalyst-loaded activated carbon achieved the PPDs of 424 and 465 mW cm<sup>-2</sup> at 850°C, respectively.<sup>39</sup> The single cell was a tubular cone-shaped Ni-based anode-supported SOFC with YSZ electrolyte and LSM cathode.<sup>39</sup> In addition, it is worth noticing that all the examples mentioned above used the silver paste as sealing material. However, at higher test temperatures, such as 850°C, the silver in the solidified silver paste can diffuse into the electrode to certain extent and may positively influence the electrochemical performance of the fuel cell because of the electrocatalytic activity of silver.

As seen in Table 2, the fuel cell operating on PCC exhibited a higher open circuit voltage (OCV) than the cell running on PC at corresponding temperature. This can be understood via the Nernst equation (5), ie, the theoretical expression of the OCV of fuel cells<sup>17</sup>:

$$E = E^0 + \frac{RT}{4F} \ln \left[ P_{O_2}^c \cdot \left( \frac{P_{CO}^a}{P_{CO_2}^a} \right)^2 \right], \quad (5)$$

where  $E$  and  $E^0$  refer to the calculated and standard electro-motivated potential, respectively;  $P_{O_2}^c$  is the partial pressure of O<sub>2</sub> at the cathode; and  $P_{CO}^a$  and  $P_{CO_2}^a$  are the partial pressures of CO and CO<sub>2</sub> at the anode, respectively. Based on the formula (5), PCC with higher Boudouard gasification performance can offer a higher ratio of  $P_{CO}^a/P_{CO_2}^a$  at the anode than that given by PC, which results in a higher OCV value for PCC than that for PC.

The electrochemical impedance spectra for PC and PCC in Figure 6C,D provide further information for understanding the polarization behaviors of fuel cells with

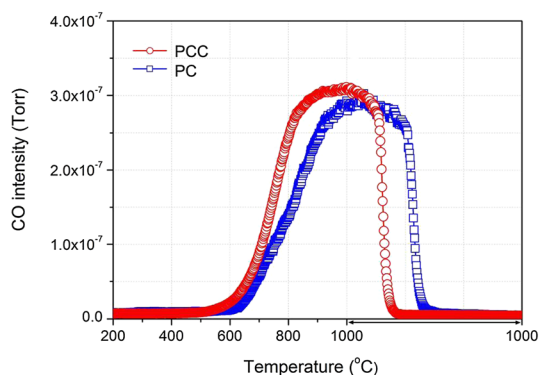


**FIGURE 5** Carbon dioxide temperature-programmed oxidation of pomelo peel char (PC) and catalyst-loaded PC (PCC) [Colour figure can be viewed at wileyonlinelibrary.com]

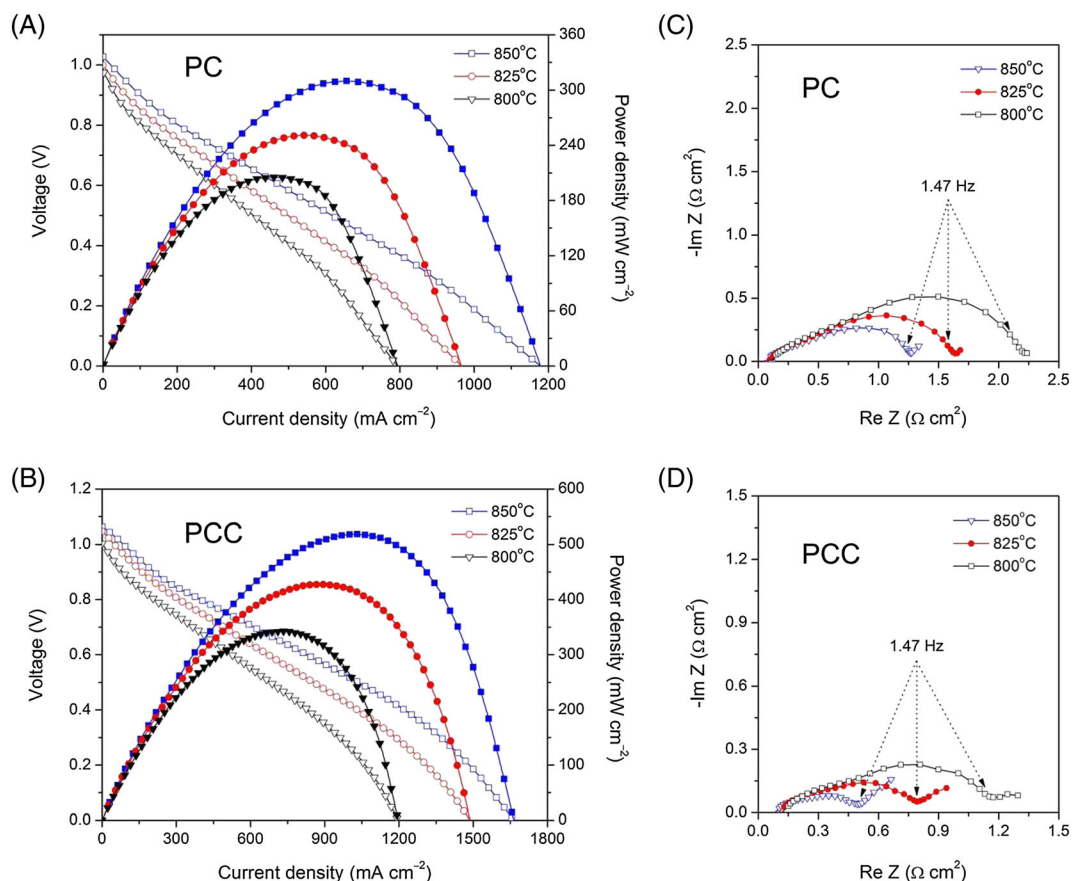


**FIGURE 6** I-V and I-P curves for the cells fed with (A) pomelo peel char (PC) and (B) catalyst-loaded PC (PCC). Electrochemical impedance spectra for: (C) PC and (D) PCC [Colour figure can be viewed at [wileyonlinelibrary.com](http://wileyonlinelibrary.com)]

decreasing temperature (ie, the I-V curves in Figure 6A,B). Combining with the data in Table 2, it can be found that the electrode polarization resistances ( $R_p$ ) increased significantly but the ohmic resistances ( $R_o$ ) increased slightly with decreasing temperature. As shown in Figure 6C,D and Table 2, the values of ohmic resistances ( $R_o$ ) are almost identical for PC and PCC at each temperature, which suggests that the electrolyte layers of the fuel cells under test were almost identical as the increase of  $R_o$  is mainly attributed to the increase of electrolyte resistance. On the other hand, the polarization resistances ( $R_p$ ) of

the cells fed with PC are nearly 2 times the  $R_p$  values of the cells fed with PCC at the same temperature. In general, under the same test condition, the cathode total polarization resistance and the anode activation resistance should be very similar for the cells fed with CO with different partial pressures. The anode mass transport resistance should be the major reason leading to this significant difference of  $R_p$ ; ie, the CO partial pressure in the anode of cells using PCC is greater than that of using PC, which is well consistent with the conclusion of the OCV analysis.

**TABLE 2** The performance of DCFCs fueled with PC and PCC

Fuel	Temperature, °C	OCV, V	PPD, $\text{mW cm}^{-2}$	Resistance, $R_T = R_o + R_p, \Omega \text{ cm}^2$		
				Total, $R_T$	Ohmic, $R_o$	Polarization, $R_p$
PC	850	1.027	309	1.335	0.106	1.229
	825	0.999	251	1.681	0.125	1.556
	800	0.974	205	2.236	0.147	2.089
PCC	850	1.064	518	0.662	0.106	0.556
	825	1.048	427	0.939	0.129	0.810
	800	1.003	342	1.295	0.149	1.146

Abbreviations: DCFCs, direct carbon fuel cells; OCV, open circuit voltage; PC, pomelo peel char; PCC, catalyst-loaded PC; PPD, peak power density.

### 3.3 | Stability of fuel cells

Figure 7A shows the results of fuel cell stability tests by using PC and PCC of 0.04 g as fuel at constant temperature of 825°C and current density of 50 mA cm<sup>-2</sup>. In Figure 7B, the test conditions were the same as those in Figure 7A except using 0.2 g fuel and an increasing operation temperature from 725°C to 775°C in a rate of 10°C hour<sup>-1</sup>. The temperature compensation effect on the gasification reactivity of solid carbons was used to alleviate the decrease of gasification reactivity of the carbon fuels. Comparing the results shown in Figure 7 A,B, it can be found that: (1) the stability of fuel cells using PC as fuel is always higher than that of using PCC. (2) By tuning the operating temperature up, a more stable operation can be realized. The results indicate that (i) PC has a relative more adequate gasification reactivity, which is more compatible with the nickel cermet anode than PCC. (3) The gasification reactivity in the initial

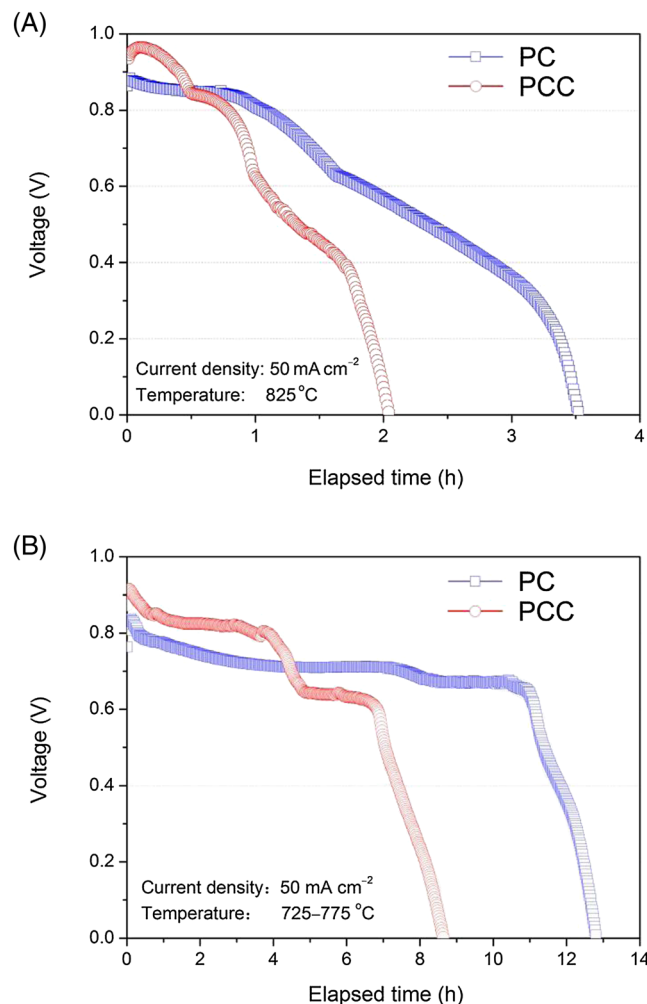


**FIGURE 7** Stability of fuel cells fed with pomelo peel char (PC) and catalyst-loaded PC (PCC) at 50 mA cm<sup>-2</sup> at (A) 825°C and (B) temperatures from 725°C to 775°C [Colour figure can be viewed at [wileyonlinelibrary.com](http://wileyonlinelibrary.com)]

stage is too high for PCC, which may result in over supply of CO to the anode, and consequently lead to the waste of fuel and more carbon deposition on the anode. At last, the quick degradation of cell's performance will occur and the fuel availability will be reduced. A post mortem analysis of the anodes was carried out to examine the carbon deposition (Figure 8), and the fuel availability was also estimated below.

The availability of PC and PCC are evaluated by the Equation (6), and the results are summarized in Table 3.

$$\eta_{\text{carbon}} = \frac{C_{\text{elec}}}{C_{\text{ld}}} \times 100\%, \quad (6)$$

where  $C_{\text{elec}}$  and  $C_{\text{ld}}$  are the masses of carbon converted electrochemically and carbon loaded in the anode chamber, respectively. As shown in Table 3, the availabilities of PC and PCC are 47.25% and 34.71%, respectively.

### 3.4 | Post mortem analysis

Figure 8A,C depicts the scanning electron microscopy images of the anode surfaces after stability test of the cells using PC and PCC as fuel, respectively, and Figure 8B,D is the corresponding EDX spectra. Although there is no obvious difference between the anode surfaces shown in the scanning electron microscopy images, the EDX spectra indicate that the quantity of deposited carbon on the anode surface of using PCC is approximately 2 times that of using PC. The underlying reason of this result could be inferred based on the Boudouard equilibrium reaction (the Equation (1)). When using PCC as fuel, the loaded catalyst promoted the Boudouard gasification of carbon to produce CO in a faster rate, which led to the increase of CO partial pressure in the anode chamber and over the anode surface. Meanwhile, if the CO supply is not consumed by the electrochemical oxidation on the anode, the excess CO will drive the Boudouard equilibrium moving to disproportionation reaction and thus result in more carbon deposition on the anode. In other words, the reason of more carbon deposition could be attributed to the nickel cermet anode for its relatively lower catalytic performance of the electrochemical oxidation of CO, which does not match the PCC fuel with higher Boudouard gasification reactivity.

The results suggest that there is a need of developing new carbon-resistant anodes with higher catalytic performance of CO electrochemical oxidation to match the solid carbon fuels with high gasification reactivity. On the other hand, the compatibility of fuels with certain anodes should be taken into account when preparing or choosing carbon fuels. Herein, the PC fuel should be

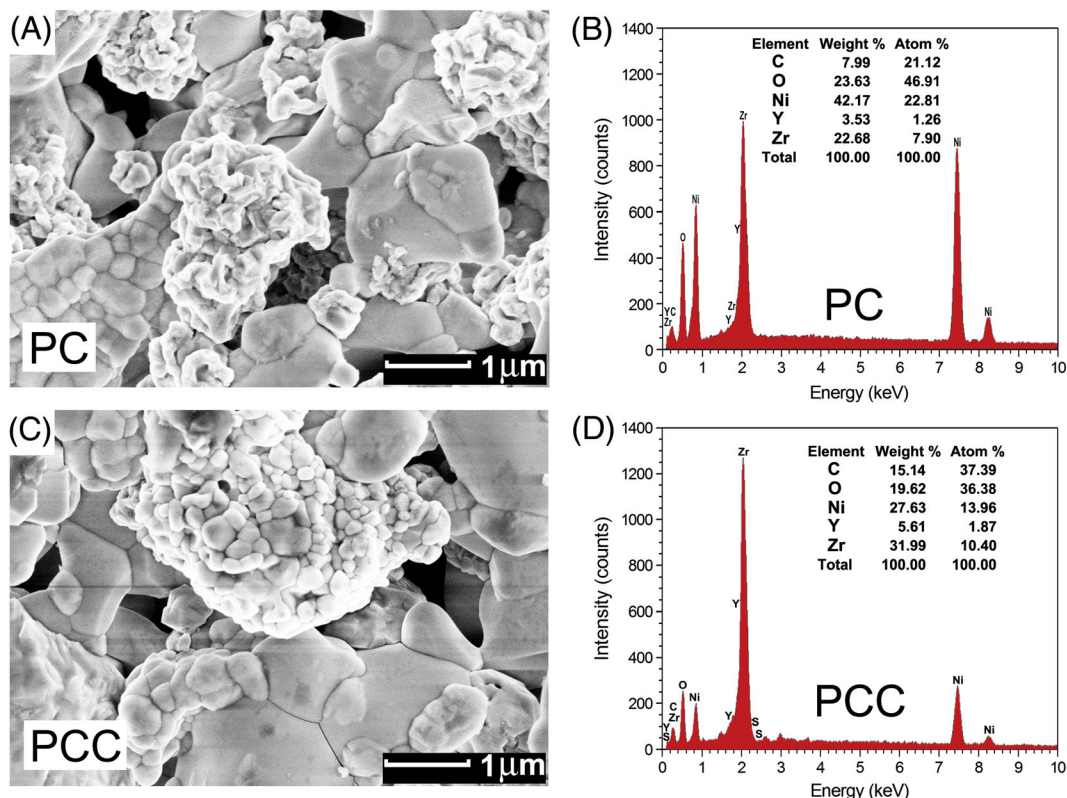


**FIGURE 8** Scanning electron microscopy images of anode surface after stability test: (A) pomelo peel char (PC) and (C) catalyst-loaded PC (PCC), and energy-dispersive X-ray spectroscopy element distribution diagrams for (B) PC and (D) PCC [Colour figure can be viewed at [wileyonlinelibrary.com](http://wileyonlinelibrary.com)]

**TABLE 3** Availability of fuel cells fed with pomelo peel char (PC) and catalyst-loaded PC (PCC)

Sample	Discharge Time, h	Electric Quantity, C	Carbon Converted, g	Carbon Loaded, g	Availability, %
PC	3.525	304.56	0.0189	0.0400	47.25%
PCC	2.046	176.77	0.0109	0.0314	34.71%

more compatible to the conventional nickel-based anode than the PCC fuel.

### 3.5 | Properties of the biomass and biochar

#### 3.5.1 | Proximate and ultimate analyses

Proximate and ultimate analyses of the sponge-like RP sample are listed in Table 4, which indicate that the RP sample is a typical carbohydrate (eg, cellulose) with the formula  $C_m(H_2O)_n$  ( $m/n = 1.27$ ). The carbon and oxygen elements account for nearly 90 wt.% of the total content,

along with a modest weight content of hydrogen element. It is worth noticing the quite low content of total sulfur ( $S_t$ , 0.05 wt.%), which is a remarkable advantage of the RP sample as a precursor of carbon fuel. In addition, the ash content is also very low.

#### 3.5.2 | Crystalline structure and chemical functional group

Figure 9A shows the XRD patterns of RP and PC. Three characteristic peaks of RP around  $2\theta = 17.1^\circ$ ,  $20.8^\circ$ , and  $34.5^\circ$  reflect the diffraction of (101), (002), and (040)

**TABLE 4** Proximate and ultimate analyses of the pomelo peel powder

Proximate Analysis, wt.%, Air Dry Basis				Ultimate Analysis, wt.%, Air Dry Basis				
M	A	V	FC	C	H	O	N	$S_t$
4.49	2.64	74.72	18.15	42.30	5.76	44.26	0.50	0.05

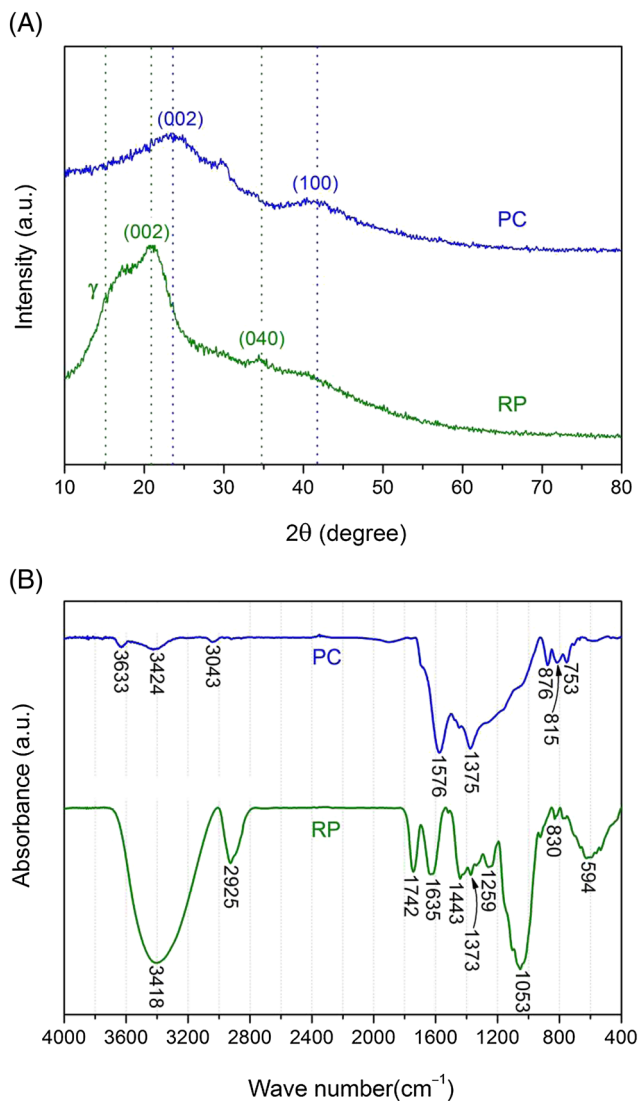


**FIGURE 9** (A) X-ray diffractogram and (B) Fourier transform infrared spectra of raw pomelo peel and pomelo peel char [Colour figure can be viewed at [wileyonlinelibrary.com](http://wileyonlinelibrary.com)]

planes of a cellulose I-type structure. A wide dispersion  $\gamma$  peak at the  $2\theta$  range from  $15^\circ$  to  $22^\circ$  attributes to the aliphatic chain reflections.<sup>29</sup> After pyrolysis treatment, the disappearance of the dispersion  $\gamma$  peak of PC indicates that the aliphatic chain structure in RP was detached or decomposed during the pyrolysis process. The XRD pattern of PC shows 2 characteristic peaks of the graphite crystal structure, ie, one higher peak around  $24^\circ$  and one lower around  $41^\circ$ , corresponding to the (002) and (100) plane reflections, respectively. In addition, a small peak at  $31.0^\circ$  might be related to the diffraction peak of certain inorganic compounds (see Section 3.5.3 the EDX results). According to the crystal structure parameter calculation, the PC has larger  $d_{002}$ , smaller  $L_a$  and  $L_c$  than those of PCC and a CC sample (Table 5), which indicates that the PC has more disordered crystal-line structure than PCC and the CC due to its smaller

**TABLE 5** Carbon microcrystalline parameters of pomelo peel char (PC) and coal char (CC)

Samples	$d_{002}$ , nm	$L_c$ , nm	$L_a$ , nm	$V_{mc}$ , nm <sup>3</sup>
PC	0.383	0.76	1.57	1.47
PCC	0.364	1.07	2.39	4.81
Coal char	0.351	4.61	1.63	9.61

crystallite size ( $L_a$  and  $L_c$ ), lower packing density ( $d_{002}$ ), and smaller microcrystal volume. The carbon microcrystal is geometrically assumed to be a cylinder, and its volume ( $V_{mc}$ ) can be estimated by the Equation (7).

$$V = \pi L_c \left( \frac{L_a}{2} \right)^2. \quad (7)$$

It is well known that the active sites of the Boudouard reaction in carbon materials are localized on the surface of the cylinder.<sup>1,17</sup> A smaller volume of carbon microcrystals means a higher proportion of surface carbon atoms to the total carbon atoms within the microcrystals. Therefore, the result suggests that the PC sample should have higher Boudouard gasification reactivity than PCC and the CC sample in their carbon microcrystalline structures.<sup>17</sup> In fact, the catalyst contained in PCC made the Boudouard gasification reactivity of PCC higher than that of PC (as discussed in Section 3.1.2). This reveals that comparing with the carbon microcrystalline structure, the catalyst of Boudouard gasification should be a more important factor influencing the Boudouard gasification performance of carbon materials.

Figure 9B shows the FTIR spectra of RP and PC to examine their surface functional groups. The main components of RP are cellulose and lignin, which contain abundant oxygenated functional groups, such as hydroxyl and carboxyl. However, only a small part of them can survive after the pyrolysis process. This is evidenced by the disappearance of many vibrational bands of RP after the thermal treatment. The intense peaks in the spectra of RP at 3418, 2925, and 1053  $\text{cm}^{-1}$  are attributed to the stretching vibrations of hydroxyl group, asymmetric and symmetric C-H stretching vibrations, and C—O—C stretching vibration or C—C framework vibration, respectively. All of them decrease sharply in the spectra of RP, indicating that the majority of oxygenated groups of RP were removed by dehydration and decarboxylation reactions. The vibration peaks of C=O, C—O, O—H, and C—O—C in the range of 1742 to 1053  $\text{cm}^{-1}$  almost disappear.

As for the FTIR spectra of PC, 2 intense peaks at 1576 and 1375  $\text{cm}^{-1}$  can be attributed to the stretching vibration of C=C and the in-plane deformation vibration of C—H, respectively. The vibration peaks at 876 and

815  $\text{cm}^{-1}$  represent the stretching vibrations of C—H bond in the aromatic rings, indicating the existence of aromatic groups. In short, the FTIR analysis reveals that the content of functional groups containing hydrogen and oxygen decreased significantly because of the decomposition of cellulose and lignin in RP. Carbon atoms in PC then rearranged into more stable aromatic carbon structures.

### 3.5.3 | Morphology and chemical element analysis

Figure 10A,C depict the morphologies of RP and PC, respectively. They are very similar and look like a

reticulated foam structure with abundant cross-connected large pores. A nitrogen adsorption analysis reveals that the specific surface area of PC is  $\sim 12 \text{ m}^2 \text{ g}^{-1}$ , agreeing well with the large pore structure. Clearly, this reticulated foam structure is beneficial for a fast mass transfer process. Figure 10E,F show the surface morphology of PC, which looks like wrinkled silk. It should be noticed that there are some fine particles distributed on the surface of PC, which might be some kind of inorganic matter.

Figures 10B and 5D show the EDX spectra of RP and PC, respectively. Compared with RP, the carbon content of PC increases from 42.79 to 76.33 wt.% with the oxygen content decreasing from 55.28 to 13.88 wt.%. Generally, the active sites of carbon fuels

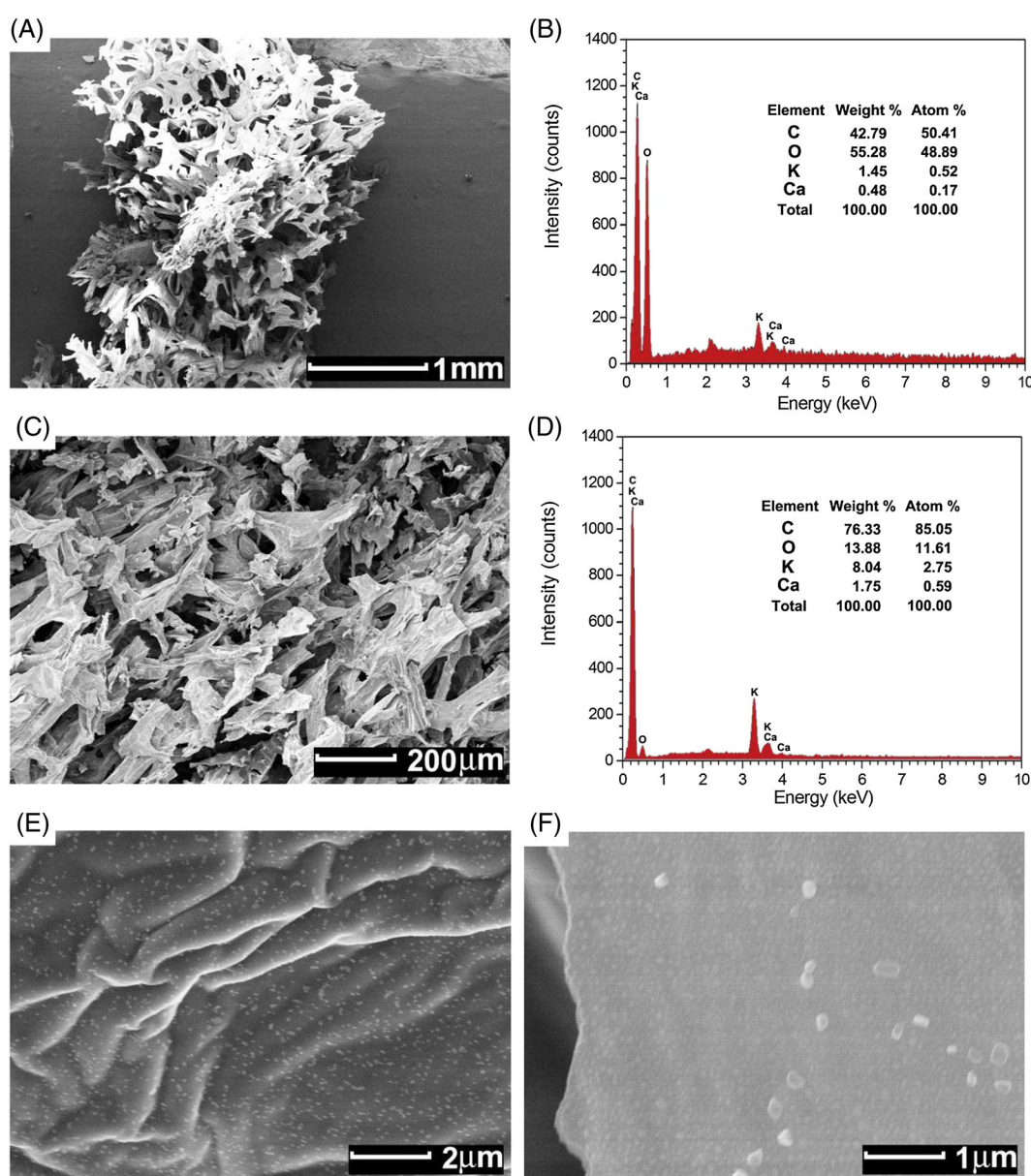


**FIGURE 10** Scanning electron microscopy images of (A) raw pomelo peel (RP), (C) pomelo peel char (PC), and element distribution diagrams for (B) RP, (D) PC, and (E and F) microstructure of PC [Colour figure can be viewed at [wileyonlinelibrary.com](http://wileyonlinelibrary.com)]

in Boudouard gasification reaction are those of oxygenated functional groups, alkyl chain residues, or atoms with dangling bonds. The oxygen content of PC remains 25 wt.% of that of RP. However, the weight ratio of oxygen to carbon of 18.2% is much higher than that of commercial activated carbon (8.8%), which suggests that there is still a large quantity of oxygenated functional groups in PC. In particular, PC contains some metal elements, such as potassium (K) and calcium (Ca), and their contents increase to roughly 5 and 4 times those in RP, respectively. K and Ca are well-known Boudouard gasification catalysts, which together with the unique microstructure of PC should endow PC an expectable high gasification activity.<sup>22,40-43</sup>

## 4 | CONCLUSIONS

The feasibility of direct use of PC as fuel for SO-DCFCs is examined. The power densities of fuel cells operating on PC and catalyst-loaded PC achieved 309 and 518 mW cm<sup>-2</sup> at 850°C, respectively. The PC exhibited superior gasification reactivity due to its unique reticulated carbon foam with homogeneously distributed inherent catalysts (K and Ca). The stability tests at a current density of 50 mA cm<sup>-2</sup> and 825°C indicated that the fuel cell using PC as fuel showed a more stable operation than that using PCC. The results suggest that PC is a promising solid carbonaceous fuel for SO-DCFCs.

## ACKNOWLEDGEMENT

This work was supported by the Shanxi Key Technologies R&D Program (20150313003-3), the Shanxi Natural Science Foundation (201601D102014), the Shanxi Coal-bed Methane Joint Foundation (2015012016), and the Shanxi Program for the Sci-tech Activities of Returnee Scholars (2014). The authors acknowledge the Australian Research Council for supporting the project under contracts DP150104365 and DP160104835. Wenting An and Yong Jiao (201608140134) would like to thank the Curtin University and the China Scholarship Council for offering a visiting scholarship, respectively.

## ORCID

Wenting An  <http://orcid.org/0000-0002-5589-2988>

Yong Jiao  <http://orcid.org/0000-0002-4947-2303>

## REFERENCES

- Cao D, Sun Y, Wang G. Direct carbon fuel cell: fundamentals and recent developments. *J Power Sources*. 2007;167(2):250-257.
- Jiang C, Ma J, Corre G, Jain SL, Irvine JTS. Challenges in developing direct carbon fuel cells. *Chem Soc Rev*. 2017;46(10):2889-2912.
- Cao T, Huang K, Shi Y, Cai N. Recent advances in high-temperature carbon-air fuel cells. *Energ Environ Sci*. 2017;10(2):460-490.
- Gür TM. Progress in carbon fuel cells for clean coal technology pipeline. *Int J Energy Res*. 2016;40(1):13-29.
- Zhou W, Jiao Y, Li S, Shao Z. Progress on anodes for carbon-fueled solid oxide fuel cells: a mini review. *ChemElectroChem*. 2015;3(2):193-203.
- Gür TM. Critical review of carbon conversion in carbon fuel cells. *Chem Rev*. 2013;113(8):6179-6206.
- Giddey S, Badwal SPS, Kulkarni A, Munnings C. A comprehensive review of direct carbon fuel cell technology. *Prog Energy Combust Sci*. 2012;38(3):360-399.
- Nakagawa N, Ishida M. Performance of an internal direct-oxidation carbon fuel cell and its evaluation by graphic exergy analysis. *Ind Eng Chem Res*. 1988;27(7):1181-1185.
- Gür TM, Huggins RA. Direct electrochemical conversion of carbon to electrical energy in a high temperature fuel cell. *J Electrochem Soc*. 1992;139(10):L95-L97.
- Xu H, Chen B, Zhang H, Sun Q, Yang G, Ni M. Modeling of direct carbon solid oxide fuel cells with H<sub>2</sub>O and CO<sub>2</sub> as gasification agents. *Int J Hydrogen Energy*. 2017;42(23):15641-15651.
- Xu H, Chen B, Liu J, Ni M. Modeling of direct carbon solid oxide fuel cell for CO and electricity cogeneration. *Appl Energy*. 2016;178:353-362.
- Xie YM, Tang YB, Liu J. A verification of the reaction mechanism of direct carbon solid oxide fuel cells. *J Solid State Electrochem*. 2013;17(1):121-127.
- Wu Y, Su C, Zhang C, Ran R, Zhao Z. A new carbon fuel cell with high power output by integrating with in situ catalytic reverse Boudouard reaction. *Electrochem Commun*. 2009;11(6):1265-1268.
- Tang Y, Liu J. Effect of anode and Boudouard reaction catalysts on the performance of direct carbon solid oxide fuel cells. *Int J Hydrogen Energy*. 2010;35(20):11188-11193.
- Li C, Shi Y, Cai N. Performance improvement of direct carbon fuel cell by introducing catalytic gasification process. *J Power Sources*. 2010;195(15):4660-4666.
- Liu R, Zhao C, Li J, et al. A novel direct carbon fuel cell by approach of tubular solid oxide fuel cells. *J Power Sources*. 2010;195(2):480-482.
- Jiao Y, Zhao J, An W, et al. Structurally modified coal char as a fuel for solid oxide-based carbon fuel cells with improved performance. *J Power Sources*. 2015;288:106-114.
- Jiao Y, Tian W, Chen H, et al. *In situ* catalyzed Boudouard reaction of coal char for solid oxide-based carbon fuel cells with improved performance. *Appl Energy*. 2015;141:200-208.
- Cai W, Zhou Q, Xie Y, et al. A direct carbon solid oxide fuel cell operated on a plant derived biofuel with natural catalyst. *Appl Energy*. 2016;179:1232-1241.
- Li X, Zhu Z, Chen J, et al. Surface modification of carbon fuels for direct carbon fuel cells. *J Power Sources*. 2009;186(1):1-9.

21. Wang W, Su C, Wu Y, Ran R, Shao Z. Progress in solid oxide fuel cells with nickel-based anodes operating on methane and related fuels. *Chem Rev.* 2013;113(10):8104-8151.
22. Karagoz S. Energy production from the pyrolysis of waste biomasses. *Int J Energy Res.* 2009;33(6):576-581.
23. Moulod M, Jalali A, Asmatulu R. Biogas derived from municipal solid waste to generate electrical power through solid oxide fuel cells. *Int J Energy Res.* 2016;40(15):2091-2104.
24. Zhu X, Li Y, Lu Z. Continuous conversion of biomass wastes in a  $\text{La}_{0.75}\text{Sr}_{0.25}\text{Cr}_{0.5}\text{Mn}_{0.5}\text{O}_{3-\delta}$  based carbon-air battery. *Int J Hydrogen Energy.* 2016;41(9):5057-5062.
25. Zhong Y, Su C, Cai R, Tadé MO, Shao Z. Process investigation of a solid carbon-fueled solid oxide fuel cell integrated with a  $\text{CO}_2$ -permeating membrane and a sintering-resistant reverse Boudouard reaction catalyst. *Energy Fuel.* 2016;30(3):1841-1848.
26. Yu J, Zhao Y, Li Y. Utilization of corn cob biochar in a direct carbon fuel cell. *J Power Sources.* 2014;270:312-317.
27. Zhou Q, Cai W, Zhang Y, et al. Electricity generation from corn cob char through a direct carbon solid oxide fuel cell. *Biomass Bioenergy.* 2016;91:250-258.
28. Methacanon P, Kongsin J, Gamonpilas C. Pomelo (*Citrus maxima*) pectin: effects of extraction parameters and its properties. *Food Hydrocoll.* 2014;35:383-391.
29. Zhou Y, Hu C, Li J. Study on the biosorption mechanism of methylene blue in aqueous solution using pummelo peel. *Res Environ Sci.* 2008;21(5):49-54.
30. Hameed BH, Mahmoud DK, Ahmad AL. Sorption of basic dye from aqueous solution by pomelo (*Citrus grandis*) peel in a batch system. *Colloids Surf A Physicochem Eng Asp.* 2008;316(1-3):78-84.
31. Zhang J, Xiang J, Dong Z, et al. Biomass derived activated carbon with 3D connected architecture for rechargeable lithium-sulfur batteries. *Electrochim Acta.* 2014;116:146-151.
32. Hong K, Qie L, Zeng R, et al. Biomass derived hard carbon used as a high performance anode material for sodium ion batteries. *J Mater Chem A.* 2014;2(32):12733-12738.
33. Sun X, Wang X, Feng N, Qiao L, Li X, He D. A new carbonaceous material derived from biomass source peels as an improved anode for lithium ion batteries. *J Anal Appl Pyrolysis.* 2013;100:181-185.
34. Chen S, Liu Q, He G, et al. Reticulated carbon foam derived from a sponge-like natural product as a high-performance anode in microbial fuel cells. *J Mater Chem.* 2012;22(35):18609-18613.
35. Liang Q, Ye L, Huang Z, et al. A honeycomb-like porous carbon derived from pomelo peel for use in high-performance supercapacitors. *Nanoscale.* 2014;6(22):13831-13837.
36. Peng H, Ma G, Sun K, Zhang Z, Yang Q, Lei Z. Nitrogen-doped interconnected carbon nanosheets from pomelo mesocarps for high performance supercapacitors. *Electrochim Acta.* 2016;190:862-871.
37. Li J, Liu W, Xiao D, Wang X. Oxygen-rich hierarchical porous carbon made from pomelo peel fiber as electrode material for supercapacitor. *Appl Surf Sci.* 2017;416:918-924.
38. Jiao Y, Zhang L, An W, et al. Controlled deposition and utilization of carbon on Ni-YSZ anodes of SOFCs operating on dry methane. *Energy.* 2016;113:432-443.
39. Bai Y, Liu Y, Tang Y, Xie Y, Liu J. Direct carbon solid oxide fuel cell—a potential high performance battery. *Int J Hydrogen Energy.* 2011;36:9198-9194.
40. Kan T, Strezov V, Evans TJ. Lignocellulosic biomass pyrolysis: a review of product properties and effects of pyrolysis parameters. *Renew Sustain Energy Rev.* 2016;57:1126-1140.
41. Perander M, DeMartini N, Brink A, et al. Catalytic effect of Ca and K on  $\text{CO}_2$  gasification of spruce wood char. *Fuel.* 2015;150:464-472.
42. Mitsuoka K, Hayashi S, Amano H, Kayahara K, Sasaoaka E, Uddin MA. Gasification of woody biomass char with  $\text{CO}_2$ : the catalytic effects of K and Ca species on char gasification reactivity. *Fuel Process Technol.* 2011;92(1):26-31.
43. Kopyscinski J, Habibi R, Mims CA, Hill JM.  $\text{K}_2\text{CO}_3$ -catalyzed  $\text{CO}_2$  gasification of ash-free coal: kinetic study. *Energy Fuel.* 2013;27(8):4875-4883.

**How to cite this article:** An W, Sun X, Jiao Y, et al. A solid oxide carbon fuel cell operating on pomelo peel char with high power output. *Int J Energy Res.* 2019;43:2514–2526. <https://doi.org/10.1002/er.4097>